Role of Water in the Ion Selectivity of Niobate-Based Octahedral Molecular Sieves

Tina M. Nenoff,*,† Nathan W. Ockwig,† Randall T. Cygan,† Todd M. Alam,† Kevin Leung,† Jason D. Pless,†,‡ Hongwu Xu,§ Monika A. Hartl,§ and Luke L. Daemen§

Sandia National Laboratories, Albuquerque New Mexico 87185-1415, and Manuel Lujan, Jr. Neutron Scattering Center, LANSCE-LC, MS-H805 Los Alamos National Laboratory, Los Alamos, New Mexico 87545

Received: May 22, 2007; In Final Form: July 9, 2007

The role of occluded water in ion exchange selectivity is examined in a class of molecular sieves named Sandia Octahedral Molecular Sieves (SOMS: $Na_2Nb_{2-x}M_xO_{6-x}(OH)_x{\cdot}H_2O$ (i.e., M = Ti; $0 < x < 0.4$)). SOMS exhibit a high selectivity for divalent cations only when the framework Nb(5+) are substituted by M(4+) atoms. Vibrational dynamics of the water molecules with varying charge balancing cations and M atoms are studied by inelastic neutron scattering (INS) measurements and ^{1}H MAS NMR and correlated to density functional theory and molecular dynamics data. The experimental INS spectra were compared with those of ice Ih to characterize the changes induced by confinement on the occluded H_2O and the resulting hydrogen-bonding network. Data indicates that, with increasing M(4+) content and divalent ion exchange, the trend of occluded water molecules is to change from extended rigid ice-like networks to restored bulk-like arrangements with increased solvation effects on the channel charge-balancing cations.

1. Introduction

Confinement in microporous materials is an attractive subject for a variety of both experimental and theoretical studies.[1−2] The case of nanoconfined water is of importance because understanding how the various confining matrices modify the water properties (compared to those in the bulk state) is of significance to the control and optimization of a broad spectrum of industrial processes. In our case, we are particularly focused on the ability to understand and, therefore, tune and predict ion exchange selectivity for water purification with zeolitic materials, especially for environmental remediation applications.

Selectivity for ion exchange in zeolites and molecular sieves is dependent on a number of factors including pore size and shape, framework composition, and surface adsorption properties.[3] In an effort to establish a comprehensive knowledge base for tuned framework design, our research is directed toward developing a structure/property relationship between zeolites and their ion exchange capabilities. In particular, we are interested in the role of the occluded water molecules. Ion selectivity and exchange have been described as resulting from a competition between the hydration free energy of a cation and the electrostatic interactions occurring in pores between crystalline framework and extraframework ions.[4] Our research is focused on a systematic study of the role of occluded water molecules in the small pored, highly selective Sandia Octahedral Molecular Sieves (SOMS).

Work on occluded water in zeolites has focused on various aluminosilicates.[5−11] In particular, these studies are directed toward understanding the arrangement of water molecules inside a zeolite cage and the interactions of that water with neighboring water molecules and the zeolite framework.[6] This includes the effects of ion exchange on the O−H stretching and H−O−H bending intramolecular vibrations and diffusional dynamics of water in zeolite A (LTA) and zeolite X with various charge balancing cations.[5] Evidence from inelastic neutron scattering (INS) and Fourier transform infrared spectroscopy (FTIR) data indicates the ability of the occluded water molecules to form structures (such as hexamers and distorted tetrahedral networks) through hydrogen bonding inside the zeolite pore. The data also indicates that the occluded water is structurally similar to bulk water. Much of the state of the water molecules was determined by the concentration of cations located in the zeolite cage.

We have applied these techniques to our SOMS ($Na_2Nb_{2-x}M_xO_{6-x}(OH)_x{\cdot}H_2O$ (ie., M = Ti; $0 < x < 0.4$)), a new class of molecular sieves that show exceptionally high selectivity for divalent cations, in particular Sr^{2+}. These phases have been synthesized using hydrothermal methods[12] and possess a framework structure composed of layers of edge-sharing $[NaO_6]$ octahedra interleaved with double chains of edge-sharing, disordered, and distorted $[NbO_6]/[MO_6]$ (see Figure 1a). The third structural unit, a square planar sodium, resides in the channels. This structure is unusual in the sense that Na^+, which is typically an extraframework cation, also participates in the framework. We have shown that, when M = Ti and $x = 0.4$, we obtain a maximum ion exchange capacity for Sr^{2+} for this framework configuration.[12] Because SOMS phases exhibit favorable distribution coefficients (K_d) for ions such as Sr^{2+}, these materials may find utility in the separation of aqueous radioactive nuclear wastes and groundwater containing species such $^{90}Sr^{2+}$. Moreover, upon heating, the Sr-exchanged SOMS phases dehydrate and convert to thermally stable and chemically durable perovskites.[12] Thus, these perovskites may serve as permanent ceramic host structures for ^{90}Sr in radioactive waste management. More recently, we reported the synthesis, structure, and thermodynamic properties of the prototypic phase, $Na_2Nb_2O_6{\cdot}H_2O$, containing only Nb (without Ti) in this system.[12] This end-member composition can be considered as a lueshite perovskite, $NaNbO_3$, with half of a water molecule per formula unit. We have also greatly expanded

* Corresponding author. E-mail: tmnenof@sandia.gov. Phone: (505) 844-0340.
† Sandia National Laboratories.
‡ Current address: Catalytic Solutions Inc., Oxnard, California.
§ Los Alamos National Laboratory.

10.1021/jp073969j CCC: $37.00
Published on Web 08/11/2007

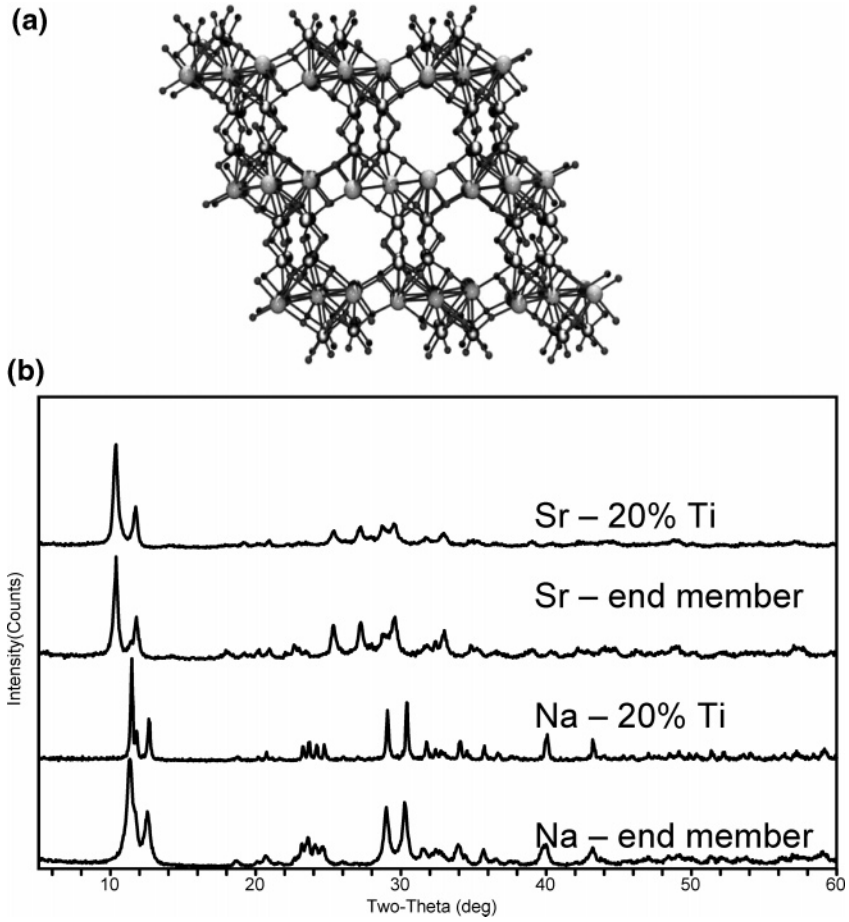

Figure 1. (a) SOMS framework, $Na_2Nb_{2-x}M^{IV}_xO_{6-x}(OH)_x \cdot H_2O$; small balls = O, medium balls = Nb/Ti, large balls = Na, occluded waters and Na(1) are not shown, for clarity, but are located in the pores. (b) Powder XRD data for the as-synthesized and Sr-exchanged samples; peak shifts due to changes in unit cell size from ion-exchanged cation size.[12b]

the phase space of SOMS to include a wide variety of occluded cations and stoichiometrically doped framework octahedral atoms.[13] The charge balancing cations include Li, Na, Sr, Mg, Ca, and Y; the octahedral framework elements (M) include Nb, Ti, Zr, Mo, Ge, and Te.

We report on the state of water in the end member SOMS ($Na_2Nb_2O_6 \cdot H_2O$) and the 20%-Ti SOMS ($Na_2Nb_{1.6}M_{0.4}O_{5.6}(OH)_{0.4} \cdot H_2O$), ranging in characteristics from bulk to ice-like ("ice-like" refers to a pore-constrained water having some long-range order and limited hydrogen bonding). Both phases were synthesized with monovalent Na^+ and ion exchanged with divalent Sr^{2+}. The state of the confined water was determined by inelastic neutron scattering and ^1H magic angle spinning (MAS) NMR experiments. Furthermore, we have correlated the experimental data with molecular simulation efforts including first principles density functional theory (DFT) with ab initio molecular dynamics and large-scale molecular dynamics modeling. An overall picture of the equilibrium dynamics is obtained through the comparative analysis and correlation of theoretical power spectra with observed spectroscopic evidence from material and crystallographic characterization, MAS NMR, inelastic neutron scattering and modeling−simulation techniques. The combined efforts allow us to postulate on the role of confined water on ion exchange capacity of a molecular sieve framework.

2. Experimental Section

The SOMS samples were all prepared according to methods published earlier.[13] Deuteration of samples was performed by repeated refluxing in D_2O (3 × 24 h). Ion exchange of the samples with Sr was performed by refluxing the as-synthesized SOMS sample with 10 wt % $Sr(NO_3)_2$ at 90 °C for 12 h. Elemental analysis was performed by inductively coupled plasma−optical emissions spectroscopy (ICP−OES) at Galbraith Laboratories, Inc., for all of the products and showed complete exchange of the sodium for strontium.

Ion exchange capacity, represented as the distribution coefficient, K_d, was calculated by the following relationship:

$$K_d\ (\text{mL/g}) = ([\text{Sr}_{ix}]/g_{ix})/([\text{Sr}_{sln}]/\text{mL soln}) \qquad (1)$$

where K_d is the distribution coefficient, ix is ion exchanger, $[Sr_{ix}]$ is the concentration of Sr adsorbed by the ion exchanger, g_{ix} is the weight of the SOMS ion exchanger, $[Sr_{sln}]$ is the concentration of the Sr remaining in solution after contacting SOMS, and mL soln is milliliters of solution.

Powder X-ray diffraction (XRD) patterns were recorded at room temperature (RT) using a Siemens Kristalloflex D 500 diffractometer (Cu Kα radiation, Kevex detector, 40 kV, 30 mA; $2\theta = 5-60°$, 0.05° step size and 3 s count time) and used for crystalline phase identification. The phases were identified by comparison with the data reported in the Joint Committee on Powder Diffraction Standards (JCPDS) database and our previous publications.[12−14]

Variable temperature time-of-flight (TOF) neutron data was collected at the neutron powder diffraction (NPDF) beamline at the Manuel Lujan, Jr. Neutron Scattering Center of Los Alamos National Laboratory (LANSCE). Prepared powder

samples were sealed in a vanadium vessel (1 cm diameter) and rotated throughout data collection. Data at each temperature (270, 150, and 15 K) was simultaneously collected on four detector banks which were centered at $\pm 90°$ and $\pm 151°$ 2θ.

INS data were collected at the filter difference spectrometer (FDS) at the LANSCE facility. This instrument is used for vibrational spectroscopy through incoherent inelastic neutron scattering. The instrument is designed for high count rates by use of a large solid-angle (3 steradians) detector. Several grams of the sample were loaded in cylindrical aluminum cans (20 mm diameter, 100 mm height) in a helium glovebox. Helium gas was used to ensure good thermal contact with the powder during subsequent cooling of the sample and sample holder to 10 K. The samples were then cooled to 10 K in a closed-cycle refrigerator, and data collection was started.

The ^{1}H MAS NMR experiments were performed on a Bruker Avance instrument at an observe frequency of 600.14 MHz. The MAS NMR experiments were performed on ~10 mg of sample using a 2.5 mm rotor with spinning speeds between 20 and 30 kHz. The chemical shifts, line widths, and relative amounts were all obtained from analysis of the 30 kHz spinning speed spectra. The two-dimensional (2D) double quantum (DQ) side band experiments and analysis of distributions have been detailed elsewhere.[15−18] Chemical shifts were referenced to a secondary sample of adamantane ($\delta = +1.63$ ppm wrt TMS $\delta = 0.0$ ppm).

Short (3 ps) DFT-based ab initio molecular dynamics (AIMD) trajectories, followed by geometric optimizations, were performed to explore the potential energy landscape of fully hydrated end-member SOMS and SOMS with ~20% Ti substitution (both with and without Sr^{2+} exchanging for Na^+). These simulations involved a single formula unit fixed at the experimental lattice constants[12a]. DFT and AIMD calculations applied the Perdew−Burke−Ernzerhof (PBE) functional[19] and projected augmented wave[20] pseudopotentials implemented into the VASP code,[21,22] $1 \times 2 \times 1$ Monkhorst−Pack Brillouin zone sampling, and a 400 eV wavefunction cutoff. The VASP Born−Oppenheimer AIMD simulations enforced a 10^{-6} eV convergence criterion at each of the 0.5 fs time step and applied a thermostat that maintained an elevated simulation temperature, $T = 900$ or 600 K, to ensure that the relatively short trajectories led to significant sampling of water configurations.

Large-scale molecular dynamics simulations were performed on the end member SOMS ($Na_2Nb_2O_3 \cdot H_2O$) and 20% Ti-substituted SOMS ($Na_2Nb_{1.6}Ti_{0.4}O_{5.6}(OH)_{0.4} \cdot H_2O$; and their corresponding Sr-exchanged phase) using the Cerius^2 software package (Accelrys Inc., San Diego) and an energy force field based on the flexible simple point charge (SPC) water model[23,24] with compatible Lennard-Jones parameters for the Na and Sr channel cations.[25] Partial charges of Na = 0.467, Nb = 3.000, Ti = 2.325, O = −1.200, O (hydroxyl) = −0.950, and H (hydroxyl) = 0.425 were assigned to the framework atoms, while charges for the channel cations (Na^+ and Sr^{2+}) were equivalent to their formal charges. Development of Nb−O interatomic parameters proved unsuccessful and limited our simulations to systems where the framework atoms were constrained to the observed structure[12] while allowing full flexibility and translation for the water (and hydroxyls) and channel cations. Intermolecular interactions consisted of electrostatics and the short-range Lennard-Jones terms from the literature, while the intramolecular interactions included bond stretch and angle bend terms based on the SPC water model. Lorentz−Berthelot mixing rules[26] were used to combine the Lennard-Jones parameters for the various framework-channel interactions. Simulations used supercell models having $P1$ symmetry and comprised of $2 \times 4 \times 4$ unit cells of the SOMS observed structure.[12] A series of molecular dynamics simulations were completed for an initial equilibration period of 100 ps, using a 1 fs time step, followed by a longer 500 ps simulation period. Atomic positions and velocities were saved every 2 ps for analysis. Additional trajectories for a subsequent 40 ps simulation were used for the velocity autocorrelation function (VACF)[27] and power spectra calculations. All simulations were conducted in the *NVT* ensemble with $T = 300$ K and used an Ewald summation to ensure proper convergence of the electrostatic energies. The thermostat relaxation time was 0.1 ps, and the Verlet velocity algorithm was used to ensure accurate integration of the equations of motion. No differences were observed in the peak positions and peak shapes for the power spectra derived using various starting configurations from the equilibrated trajectories. Uncertainties in the molecular dynamics results are ultimately dependent upon the accuracy of the empirical force field parameters; for this study, the results are consistent and in general agreement with those derived from the DFT approach.

3. Results and Discussion

The ion exchange capacity for the SOMS end member $Na_2Nb_2O_6 \cdot H_2O$ indicated low selectivity for Sr^{2+}, $K_d \approx 3800$, while the $Na_2Nb_{1.6}Ti_{0.4}O_{5.6}(OH)_{0.4} \cdot H_2O$ indicated high selectivity for Sr^{2+} ions, $K_d \approx 26\,000$. Complete ion exchange occurred for both samples, resulting in final stoichiometries of $SrNb_2O_6 \cdot H_2O$ and $SrNb_{1.6}Ti_{0.4}O_{5.6}(OH)_{0.4} \cdot H_2O$. XRD analysis indicated no degradation or change in the SOMS frameworks. See Figure 1b.

Neutron Diffraction. The first attempt to understand the characteristics of the occluded water in the SOMS included analysis of variable low-temperature neutron diffraction studies, with a focus on the oxygen atom of the occluded water molecule (O_w). The Rietveld method[28] was used to analyze the neutron TOF data using the General Structure Analysis System (GSAS) software suite developed by Larson and Von Dreele.[29] Initial unit cells and atomic positions were taken from our previous SOMS structure solution and refined as follows: Scale factors and six background terms were refined until converged, after which, specimen displacement and lattice parameters were added and optimized. An additional six background terms were added to each refinement, and peak profiles were fit to pseudo-Voigt[29] functions. Upon convergence of the above parameters, atomic coordinates and isotropic temperature factors for all atoms were refined to yield combined R_{wp}values of 2.14, 2.11, and 2.27 for 15, 150, and 270 K, respectively (Table 1).

The SOMS crystallize in a monoclinic cell with space group $C2/c$ (No. 15). The unit cell is independent of the temperature, exchanged cations, or concentration of framework dopant.[12] The parameters of the unit cell at 15, 150, and 270 K show a nearly linear expansion of the *b* axis and contraction of the *a* parameter resulting in a net increase in unit cell volume as room temperature is approached. Unlike the *a* and *b* parameters, the *c* parameter does not follow a linear behavior with temperature and exhibits a local maximum at 150 K. The thermal behavior of this material is most readily understood through comparison of the local environment surrounding sodium ions within the pores (Na3) at 15, 150, and 270 K. Na3 is four coordinate, in square-planar configuration, by two symmetry equivalent framework oxygen atoms (O_f) and two water oxygen atoms (O_w). The channel sodium-framework oxygen (Na3−O_f) interaction is parallel to the *c* parameter and has a significant contribution

TABLE 1:

temperature[a]	15 K	150 K	270 K
a (Å)	16.8814(3)	16.8562(9)	16.8294(7)
b (Å)	5.0196(7)	5.0261(1)	5.0293(4)
c (Å)	16.3731(2)	16.3849(2)	16.3758(6)
β (°)	114.059(9)	114.044(4)	114.044(2)
V (Å^3)	1269.89(7)	1271.81(3)	1275.79(8)
R_{wp} (%)	2.14	2.11	2.27
R_p (%)	1.03	1.60	1.81
χ^2	2.197	2.752	2.281
Nb1−O_f (Å)	2.0484(4)	2.0422(5)	2.0366(1)
Nb2−O_f (Å)	2.0124(9)	2.0072(7)	2.0131(3)
Na1−O_f (Å)	2.4671(6)	2.4694(1)	2.4601(2)
Na1−O_w (Å)	2.4163(1)	2.4188(4)	2.4217(1)
Na2−O_f (Å)	2.4888(3)	2.4843(1)	2.5029(2)
Na3−O_f (Å)	2.3623(1)	2.3711(5)	2.3753(3)
Na3−O_w (Å)	2.1250(6)	2.1258(4)	2.1289(9)
Na3−O_f (Å)	2.3717(7)	2.3784(2)	2.3734(3)
O1w	0.04972	0.07029	0.09001

[a] O_f and O_w indicate framework and water oxygens, respectively.

to its length. This Na−O bond length shows the same nonlinear behavior which is exhibited be the *c* parameter as room temperature is approached. Analysis of the refinement data shows that there is almost no displacement of the water positions at low temperatures and that the occluded water in the end member SOMS is not thermally labile in the range studied. Therefore, the incorporation of hydroxyl moieties through M^{4+} doping within the SOMS materials must significantly enhance the pore environment electronic structure. As we show in concurrent studies, the hydroxylated pore favors larger charged ions such as Sr^{2+} and Ba^{2+} over the smaller more highly charged ions such as Na^+ and Cs^+.[30]

Inelastic Neutron Diffraction Studies. Because of the lack of additional information on the characteristics of the O_w from low-temperature neutron diffraction data (above), INS analysis was performed to study the hydrogen bonding of the water molecule. This technique is ideally suited to investigate the librational and rotational modes (wagging, rocking, and twisting) of water molecules in confined environments and is extremely sensitive to localized hydrogen bonding. Conceptually, the behavior of nanoconfined water molecules is the direct result of complex equilibria among four distinct types of interactions: (1) H_2O-H_2O, (2) H_2O−ion, (3) H_2O−framework, and (4) ion−framework. The collective effect of these interactions (hydrogen bonds, ion−dipole, and electrostatics) produces localized restrictions which alter the behavior of the nanoconfined water. Spectroscopically, these behavioral modifications are manifested by changes in the librational and rotational (300−1100 cm^{-1}) modes and to a lesser extent the intramolecular bending (∼1600 cm^{-1}) and stretching (3300−3700 cm^{-1}) modes.[5] Water has a librational band in the 450−900 cm^{-1} region, which is normally composed of three frequencies (wagging, rocking, and twisting) in the inelastic neutron scattering spectrum. For a water molecule in a general force field, there will be three librations, one for each axis of rotation, but these will be observed only if there is a restoring force present for each libration. There is the "rock", the motion in the plane of the water molecule; the "twist", which is a rotation about the C_2 diad; and the "wag", the rotation about the H−H axis, with increasing frequency. Changes to the degree of hydrogen bonding between the occluded water molecules and between the water and the cation or the framework will be exhibited in this region. Liquid water (or more appropriately for neutron spectroscopy, ice Ih) is used as a reference for the INS studies.[31] This data was reproduced in our studies at LANSCE (see Figure 2).

As-Made Samples. The INS data for the end member and 20% Ti SOMS is shown in Figure 3. Both sets of data include hydrogen bond stretching and occluded water rotational and librational modes. However, there are two distinctly different librational patterns for the librational modes of the occluded water (one per unit cell, located in the pores). In the end member case, the individual librational modes are not distinguishable. Instead, the characteristic finger print of the librational edge of ice Ih is evident at ≈ 550 cm^{-1}. Contrary to that data, the 20% Ti SOMS data have very well-defined librational peaks, visible at ≈ 533, 654, and 785 cm^{-1}. When a deuterated sample of the 20% Ti SOMS is studied, there are noticeable changes (a decrease) to the relative intensity of the librational peaks; however, peak position has not changed. The decrease in relative intensity is very informative. First, it indicates only one type of proton environment has been exchanged in the deuteration process, and that is the proton associated with the occluded water molecules that are able to exhibit the librational transitions. Second, the invariance of the other bands (e.g., the hydrogen-bonding modes of the metal−water bands in the 150 cm^{-1} region) further confirms only the occluded solvating waters are involved.

Sr-Exchanged Samples. The INS data for the fully exchanged Sr end member ($SrNb_2O_6 \cdot H_2O$) and the Sr-exchanged 20% Ti SOMS ($SrNb_{1.6}Ti_{0.4}O_{5.6}OH_{0.4} \cdot H_2O$) have been collected and are compared to their nonexchanged versions. In the Sr-exchanged end member data, the once sharp distinct Ih peak has been lost, and a very broad, featureless hump is now evident (centered at ≈ 450 cm^{-1}). A shift to ≈ 300 cm^{-1} in the metal−water modes is also observed. In contrast, the Sr-exchanged 20% Ti SOMS has only minor changes to the data. There is a noticeable shift to lower frequencies in the librational modes to ≈ 503, 604, and 759 cm^{-1} and a significant broadening of the peaks. The slight shift to lower frequencies may be due to the larger sized cations (Sr^{2+} as compared with the Na^+ cations) and the presence of framework hydroxides (−O_fH) both inhibiting hydrogen bonding among water molecules in the pores.[29]

In the case of the Sr-exchanged end member SOMS, we see distinctly different INS spectra. In the as-made end member, the pores contain one Na and one water per unit cell. There is little spatial interference with the water molecules forming hydrogen bonds with each other along the one-dimensional channel of the SOMS. Contrasting that is the Sr-exchanged end member, with 50% of the unit cells having one water and one dangling hydroxide (attached to the framework)[12b] and the other 50% having one water, one dangling hydroxide, and one strontium ion. It is possible to view the occluded water in this phase as having segregated into two distinct networks of water molecules: one network has a charge balancing Sr^{2+} present, while the other network has no cation present. Each network has water that is hydrogen bonded, but there may not be hydrogen bonding interactions between the two networks. The librational modes for each network tend to merge into a very broad, very intense continuum, and the librational edge shifts to lower frequencies if one of the networks is more loosely held together than the other.

Another possible explanation is the loss of long-range order in the network(s) of hydrogen-bonded water molecules. Short-range ordering of the water molecules is preserved (e.g., around a particular cation), but there is no long-range order throughout the structure. The resulting network of bonds of various length, strength, and orientation causes a broadening of the librational levels and a loosening of the librational motion (hence the shift

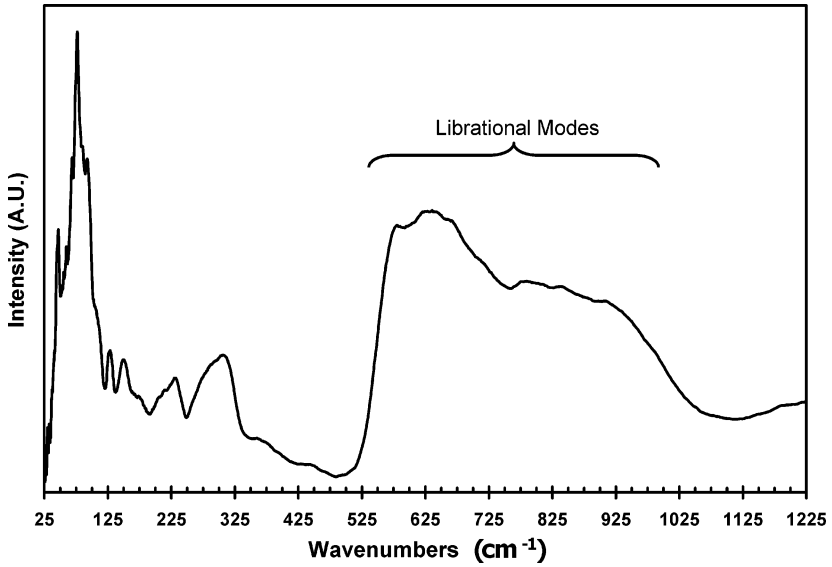

Figure 2. INS spectrum of water collected at 10 K.

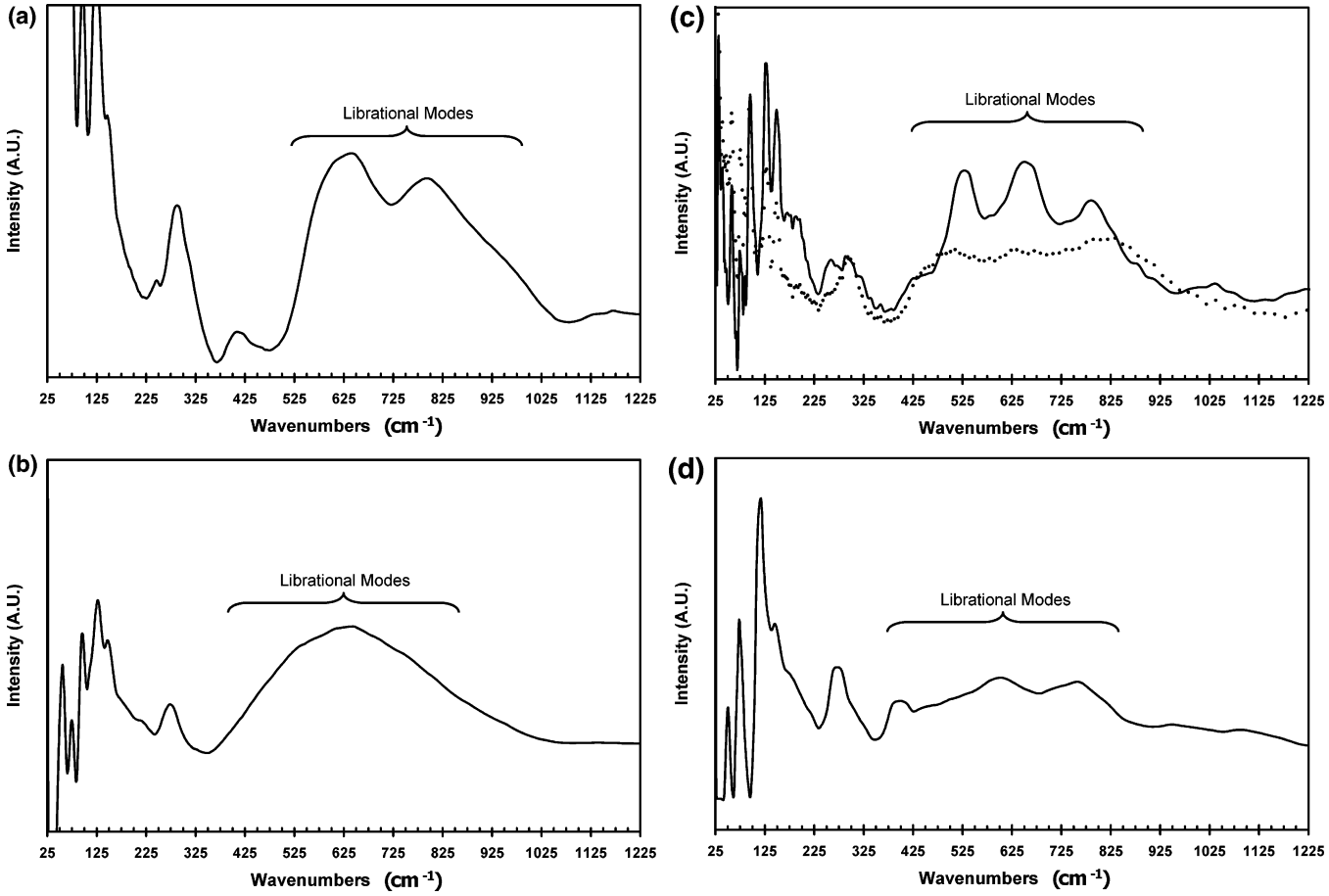

Figure 3. INS data collected at 10 K for (a) SOMS end member, ice-like peak at ≈550 cm^{-1}; (b) Sr-exchanged SOMS end member, librational modes at ≈450 cm^{-1}; (c) 20%Ti SOMS, librational modes of water at 533, 654, and 785 cm^{-1} (decreased intensity data dotted line is ^2H sample); (d) Sr-exchanged 20% Ti SOMS, librational modes at 503, 604, and 759 cm^{-1}.

of the librational edge to lower frequencies). The shift of the librational edge to a lower frequency is typically due to weakening of the O−H···O bending force constant.[32]

It is possible that the above situations (two networks of hydrogen bonds or loss of long-range order) can occur simultaneously. This is the case in high density amorphous ice, the structure of which can be thought of as two interpenetrating, but noninteracting hydrogen-bonded water networks. Each has significant density of structural ions, molecules, and pore bonded hydroxyls that cause a loss of any kind of long-range order in the translational and rotational ordering of the water molecules. MAS NMR studies have been employed to help clarify the explanation of these hydrogen-bonding networks in the Sr-exchanged phases (see below).

^{1}H MAS NMR. To further probe the local environment of these water molecules and the water dynamics on the micro- to millisecond time scale, ^{1}H MAS NMR techniques were utilized. The ^{1}H MAS NMR spectrum of end member $Na_2Nb_2O_6 \cdot H_2O$

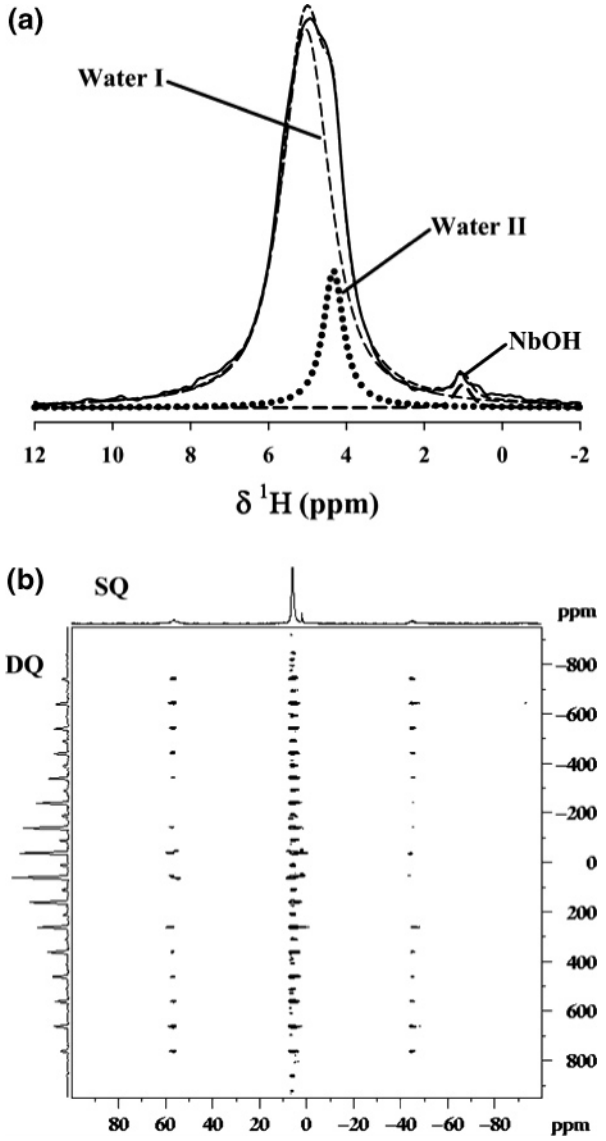

Figure 4. (a) ^{1}H MAS NMR of the end member $Na_2Nb_2O_6{\cdot}H_2O$ material revealing three overlapping proton species, including the dominant rigid water species (Water I), a mobile water species (Water II), and the NbOH hydroxyl. The (b) 2D DQ 1H MAS NMR correlation experiment where the multiple DQ spinning sidebands (left projection) can be used to determine the effective dipolar coupling of the immobile water species.

(see Figure 4a) revealed three overlapping proton species with the major (90% relative concentration) resonance at $\delta = +5.0$ ppm, (full width at half-maximum line width, fwhm = 892 Hz) due to an immobile water environment, a second ^{1}H resonance (9%) at $\delta = +4.3$ ppm (fwhm = 378 Hz) due to a mobile water environment, along with the minor (~1%) NbOH species at $\delta = +1.0$ ppm (fwhm = 300 Hz). These ^{1}H assignments are based on previous studies of niobate materials,[16,17] double quantum filtered (DQF) experiments,[18] along with the residual dipolar interaction strength measured using the 2D DQ correlation experiments described below. For the 20% Ti SOMS $Na_2Nb_{1.6}Ti_{0.4}O_{5.6}{\cdot}H_2O$ material, only a single resonance at $\delta = +4.7$ ppm (fwhm = 450 Hz) was observed in the ^{1}H MAS NMR spectrum (Figure 1S, in Supporting Information).

The extent of spinning sidebands (SSB) in the ^{1}H MAS NMR spectra of these different materials provides a qualitative measurement of the effective homonuclear ^{1}H−^{1}H dipole coupling present for these different water species. In a rigid (totally immobile) water molecule, the ^{1}H−^{1}H dipolar coupling ($D^{ij}_{\text{rigid}}/2\pi$) is on the order of 33.4 kHz, producing numerous SSB in the ^{1}H MAS NMR spectra.[15−18] If there are water dynamics that are rapid compared with this ^{1}H−^{1}H dipolar coupling coupling ($\ll 30\ \mu$s) then an averaging of the dipolar coupling will occur, reducing the number and intensity of the SSB observed. Comparison of the ^{1}H MAS NMR spectra for these two Na-containing samples indicates that the majority of the waters ($\delta = +5.0$ ppm) in the $Na_2Nb_2O_6{\cdot}H_2O$ end member are relatively immobile (see Figure 2S, Supporting Information), while the water species in the 20% Ti SOMS are mobile enough to produce significant averaging of the ^{1}H−^{1}H dipolar coupling and reduction of the SSB (see Figure 1S, Supporting Information).

2D DQ ^{1}H MAS NMR correlation experiments were also performed to directly measure the mobility of the occluded water molecules in the end member $Na_2Nb_2O_6{\cdot}H_2O$ material (Figure 4b). By analyzing the SSB patterns in the DQ dimension (left projection in 4b) from these 2D NMR experiments, an accurate measurement of the residual ^{1}H−^{1}H dipolar coupling and related distribution of dipolar coupling strengths for waters can be measured.[15,17] The effective dipolar coupling found for the rigid water species in the end member material was 28 ± 0.5 kHz, with a distribution of $\sigma \approx 4$ (±1) kHz. This corresponds to a water order parameter of $S_{H_2O} = D^{ij}_{\text{eff}}/D^{ij}_{\text{rigid}} = 28$ kHz/33.4 kHz = 0.84. This DQ measurement shows that this water environment is relatively immobile within the material even at or above RT. By comparison, the 20% Ti SOMS compound has almost all waters filtered out during the DQ experiments (Figure 2S, Supporting Information), consistent with a residual dipolar coupling <3 kHz, indicating that for this compound all of the water environments have a higher degree of mobility.

The same type of ^{1}H MAS NMR experiments can also be performed on the Sr-exchanged materials. The NMR of the $SrNb_2O_6{\cdot}H_2O$ compound reveals (Figure 5a) two broad resonances at $\delta = +6.1$ ppm (~55%, fwhm = 1300 Hz) and at $\delta = +8.3$ ppm (~45%, fwhm = 2020 Hz), plus a small NbOH resonance at $\delta = 2.2$ ppm (~5%, fwhm = 390 Hz). This ^{1}H MAS NMR spectra is very different from the nonexchanged $Na_2Nb_2O_6{\cdot}H_2O$ sample. In general, there is an increase in the observed ^{1}H NMR chemical shifts following the Sr exchange suggesting subtle changes in the local partial charge of the framework environment. Also of interest is the appearance of a water environment with an increased chemical shift ($\delta = +8.3$ ppm)[17] following Sr exchange that results from either a change in the available surface charge of the cage structure, a reduction in the rapid exchange between acid and bulk type H_2O environments, or a change in the local water confinement. Figure 5b shows the full expansion of the ^{1}H 1D MAS NMR spectrum revealing numerous SSB for this resonance even at 30 kHz spinning speeds. Note that only SSB for the Water I species are observed (inset Figure 5b), consistent with these water environments being relatively immobile. Figure 5c shows the overlap between the 1D DQF ^{1}H MAS NMR spectra and the direct ^{1}H MAS NMR spectra. Inspection of this figure shows that the Water I resonance ($\delta = +8.3$ ppm) has the largest dipolar coupling (thus surviving the DQ filter), also consistent with an immobile water species. In contrast, the $\delta = +6.1$ ppm water species does not show SSB, nor does it survive the DQ filtering (Figure 5c), and is therefore is described as mobile on the NMR time scale. The 2D DQ ^{1}H MAS NMR sideband analysis for the Water I resonance ($\delta = +8.3$ ppm) gives $D^{ij}_{\text{eff}} \sim 25 \pm 0.5$ kHz, $\sigma = 7$ (±1) kHz. ($S_{H_2O} = 0.75$), and is slightly smaller than that observed for the nonexchanged material, implying very similar water dynamics, but has an increased

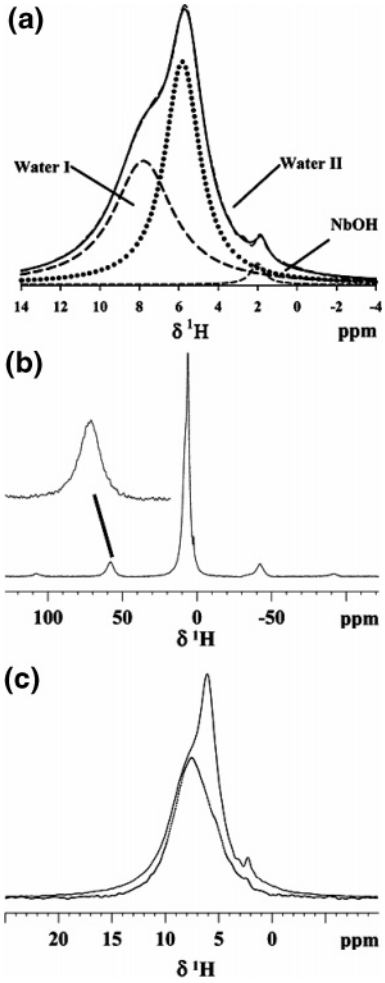

Figure 5. (a) Isotropic chemical shift region of the ^{1}H MAS NMR for the end member $SrNb_2O_6 \cdot H_2O$ material revealing three overlapping proton species, including the possible immobile water species (Water I), a mobile water species (Water II), and the NbOH hydroxyl. The (b) full ^{1}H MAS NMR spectrum showing the presence of significant sidebands for only the Water I resonance (inset) even at a 30 kHz spinning speed. The (c) DQ-filtered (lower) and direct polarization ^{1}H MAS NMR spectra clearly showing that only the Water I resonances are present following the DQ filtering, while the Water II species is suppressed.

distribution of dipolar couplings (motion types). Similarly, the ^{1}H MAS NMR spectrum for the $SrNb_{1.6}Ti_{0.4}O_{5.6}OH_{0.4} \cdot H_2O$ compound revealed two broad resonances at $\delta = +8.4$ ppm ($\sim$ 28%, fwhm = 2130 Hz) and $\delta = +6.2$ ppm ($\sim$70%, fwhm = 1975 Hz). Again, on the basis of the intensity of the SSB in the ^{1}H MAS NMR spectrum, along with the results of the DQF experiments, the $\delta = +8.4$ ppm water environment has the lowest degree of mobility, $D_{\mathrm{eff}}^{ij} \sim 28 \pm 1$ kHz, $\sigma = 8$ (± 1) kHz. ($S_{H_2O} = 0.84$), while the $\delta = +6.2$ ppm resonance has a high degree of mobility.

Comparisons between the two Sr-exchanged phases reveal that the concentration of mobile water ($\delta \sim 6$ ppm) increases with the addition of Ti. This correlates well with the INS data. Comparison between the Sr and the as-synthesized Na phases shows that the Sr exchange resulted in a portion of the occluded nonmobile water becoming mobile in the $NaNb_2O_6 \cdot H_2O$ end group. In the 20% Ti SOMS material, the Sr-exchange materials result in a fraction of the water species remaining immobile in comparison with the nonexchanged 20% Ti SOMS. The $NaNb_2O_6 \cdot H_2O$ end member has the most free volume in the pore allowing the occluded water to form H-bonding networks and a higher concentration of ice-like water formations. Either as the number of pore ions decreases because of divalent cation exchange, or as the addition of dangling pore $-$OH increases because of framework substitution (i.e., Ti doping in framework), or as both occur, the occluded water H-bonding network is interrupted and ice-like water is not formed.

A brief comment on the types of water motions that can lead to the averaging of the ^{1}H$-^1$H dipolar coupling is warranted. As previously discussed,[17] isotropic motions that would be expected for bulk water solutions completely average the ^{1}H$-^1$H dipolar coupling giving rise to $S_{H_2O} \sim 0$. This type of dipolar coupling averaging is observed for the water environments we have designated as "mobile" species. Another proposed motion is the continuous spinning of the water molecule around the molecular C_{2v} symmetry axis, which will give a water dipolar order parameter of $S_{H_2O} \sim 0.5$. The observation of dipolar order parameters for the "immobile" water environments between 0.74 and 0.84 precludes this type of rapid spinning motion. On the other hand, discrete 180° jumps around the molecular C_{2v} symmetry axis will not average the ^{1}H$-^1$H dipolar coupling because this motion produces co-incident dipolar tensors and is therefore not detectable using the ^{1}H$-^1$H DQ NMR experiments.[17] The experimental S_{H_2O} values slightly reduced from unity suggest that librational-type water motions are present (in addition to the possibility of discrete 180° flips) giving rise to partial averaging of the ^{1}H$-^1$H dipolar coupling.

Density Functional Theory. We performed DFT calculations for the undoped end member SOMS in a unit cell containing 16 Nb, 16 Na, and 48 O atoms. Analogous simulations were performed for two 18.75% Ti-substituted unit cells, with stoichiometries $Na_{16}Nb_{13}Ti_3O_{45}(OH)_3$ and $Na_{12}Sr_4Nb_{13}Ti_3O_{45}(OH)_3$, respectively. Since it was found that varying the Ti concentration has little effect on the lattice constants,[12b] all calculations were performed at the experimental lattice constants derived for 20% Ti SOMS.[12a] All simulation cells contain 8 H_2O molecules. By performing AIMD simulations and then applying geometric optimization, we sought to investigate the changes in the potential energy landscape for water induced by the Ti and Sr substitution. Despite the relatively small cell size and short trajectories mandated by DFT calculations, the accuracy of DFT methods, particularly when applied to Ti substitution, makes this a worthwhile approach that enables qualitatively comparisons with experiments and classical force field MD simulations (see below).

First, we considered the end member SOMS. To initiate geometric optimization, the SOMS framework atoms and the oxygen sites of eight water molecules were placed at the X-ray determined positions,[12] while the water protons were oriented to form hydrogen bonds to framework oxygen atoms. The optimal structure is depicted in Figure 6a. In this ordered structure, two water molecules coordinate to each Na atom located at the center of the SOMS channels or pores. Each H_2O is also coordinated to another framework Na, in addition to forming two hydrogen bonds with framework oxygen atoms. To further demonstrate that this water configuration is robust and independent of the initial configuration, we conducted a 3 ps AIMD simulation starting from the structure in Figure 6a, with the trajectory maintained at $T = 900$ K to accelerate water motion and sampling of their energy landscape. When the final configuration in this trajectory was re-optimized, the same stable structure (Figure 6a) with identical total energy was recovered. While not definitive, this strongly suggests that the water structure predicted from DFT calculations is a stable global minimum.

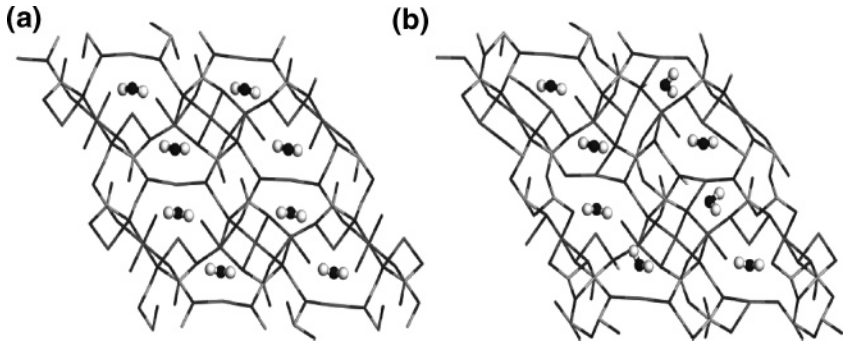

Figure 6. DFT optimized SOMS unit cell. The framework atoms are shown in wireframe, and the water are depicted as ball-and-stick models. (a) 0% Ti, (b) 18.75% Ti.

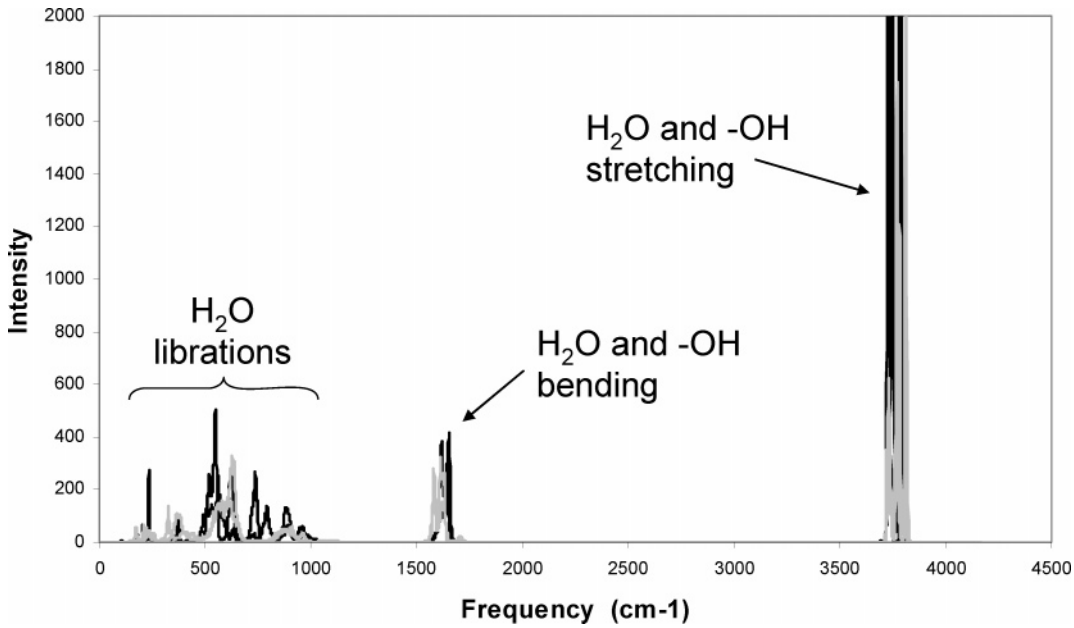

Figure 7. Comparison of entire power spectra derived from molecular dynamics simulations for all modes of water and hydroxyl in Na−SOMS and Na−Ti−SOMS (black) and Sr−SOMS and Sr−Ti−SOMS (gray).

We also considered SOMS structures where we randomly replaced three of the Nb atoms with Ti, and one of the O coordinated to each Ti with OH to preserve charge neutrality; this is a mimic for the 20% Ti SOMS. In one structure, Sr^{2+} substituted for the Na^+ in two of the four channels in the SOMS unit cell; to maintain charge neutrality and in accordance with experiments, the remaining Na^+ in the other two SOMS channels were also removed. No Sr^{2+} was included in the other Ti-substituted structure.

For a Sr-free, Ti-substituted system, performing geometry optimization from the X-ray positions led to water configurations that are less well-ordered than the end member SOMS. Some water molecules become preferentially coordinated to the hydroxyl groups in the framework instead of the pore center Na. See Figure 6b. We also conducted AIMD at $T = 900$ K starting from this configuration and re-optimized the geometry from snapshots taken 1.5 and 3.0 ps into this trajectory. The resulting water configurations are again disordered but are considerably different from those in Figure 6b. Despite this, these two configurations quenched from high temperature are only 0.16 and 0.26 eV per formula unit higher in energy than the one directly optimized from X-ray structures. These heat-and-quench numerical "experiments" demonstrate that the addition of Ti dopants lead to metastable structures which are local minima in the energy landscape with very similar energies. The results and conclusions for Sr-exchanged, Ti-substituted SOMS (not shown) are similar.

These DFT results are consistent with the experimental finding that water is more mobile in Ti-substituted SOMS and in the Sr-exchanged SOMS than in the as-synthesized end member system and that water is predominantly solvating the cations in the pores. In the absence of Ti, the water configuration is highly ordered and stable. The introduction of Ti dopants lead to disordered water structures and the existence of multiple local minima in the energy landscape, which should in turn lead to faster water librational and diffusive motion.

Molecular Dynamics Simulations. An overall picture of the equilibrium dynamics for the various SOMS materials can be obtained through the comparative analysis and correlation of power spectra (derived from the classical molecular dynamics simulations) with observed spectroscopic evidence from inelastic neutron scattering and NMR techniques.

Power spectra are derived from velocity auto correlation functions (VACF) and large scale molecular dynamics simulations.[33−35] The atomic positions and velocities from the simulation trajectories were processed to identify correlated motions for the occluded water in all structures and the hydroxyl groups in the Ti-doped SOMS models. The time domain correlations were then Fourier transformed to obtain the frequency domain response corresponding to the power spectrum. The results

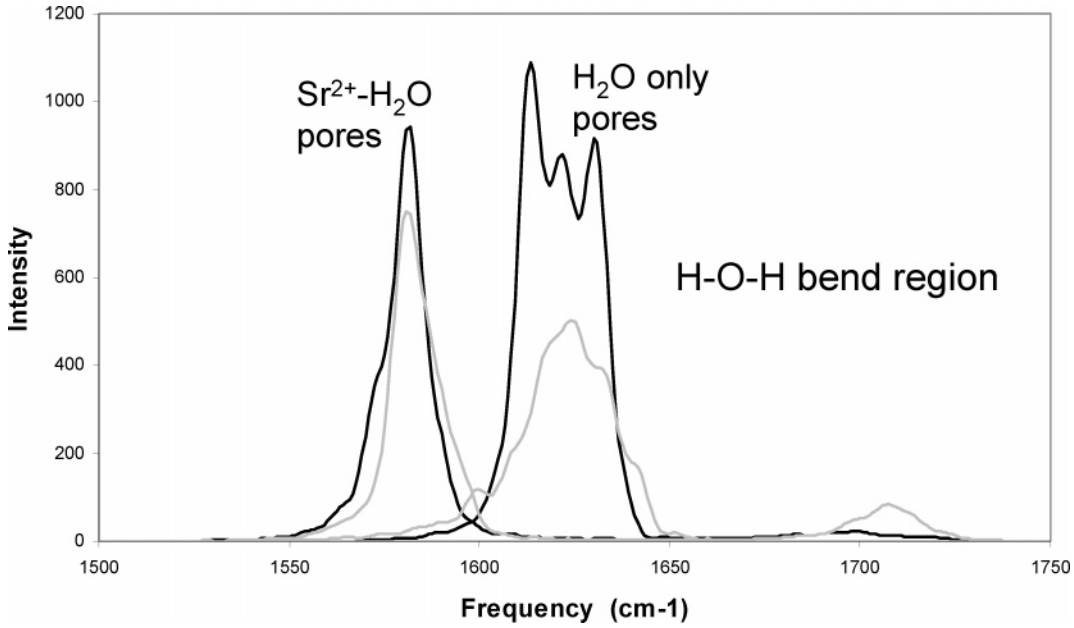

Figure 8. Comparison of power spectra derived from molecular dynamics simulations for bend modes of occluded water in Sr−SOMS (black) and Sr−Ti−SOMS (gray) indicating difference between isolated water and Sr-associated water in channels (pores).

indicate a distinction in the bend and stretch vibrational regions between the Sr and Na SOMS that also exists for both the end member and the Ti-doped materials (Figure 7).

Significant differences in the power spectra for the SOMS structures having different pore cations are clearly observed (Figure 7). Power spectra for the Na SOMS exhibit a shift ($\approx$ 50 cm^{-1}) of the bend (deformation) peaks to higher frequencies (relative to the Sr SOMS) and a shift ($\approx$ 50 cm^{-1}) of the stretch peaks to lower frequencies. The models also suggest that substitution of Ti for Nb for either Na or Sr SOMS leads to similar shifts of the power spectra and a more liquid-like environment in the channel, consistent with the DFT results. In part, this response is related to the charge compensating hydroxyl group that contributes to the formation of a more stable hydrogen-bonded configuration. However, it is important to emphasize that the small highly charged ions such as Sr^{2+} are less polarizable than the monovalent Na^+ and have larger hydration energies. In such a case, water−ion interactions dominate over the weaker water−SOMS and water−water interactions and therefore have the strongest influence on occluded water properties.

In general, the power spectra results, which are consistent with INS vibrational spectra and NMR observations, indicate channel water behaves differently depending on the channel cation; the water may be more constrained for ions like Na^+ and more liquid-like for Sr^{2+} as the channel cation. Additionally, atomic trajectories obtained from the simulations for $SrNb_2O_6 \cdot H_2O$ and $SrNb_{1.6}Ti_{0.4}O_{5.6}(OH)_{0.4} \cdot H_2O$ systems exhibit noticeable differences in the power spectra for isolated channel water compared with water associated with Sr^{2+}. The deformation (bending) region for hydroxyl ($\approx$ 1500 to 1750 cm^{-1}) is typically quite broad in the INS data relative to the more dominant modes for metal−water interactions and librational modes for water (see Figure 3). However, analysis of the power spectra clearly indicates the different environment for water in the SOMS pore with and without the exchangeable cation. The most sensitive discriminator for this behavior is found in the deformation mode of water where we observe a shift of approximately 40 cm^{-1} (see Figure 8). The exchange of divalent Sr^{2+} for Na^+ in SOMS requires only half the number of occupied channel sites and therefore generates free water that can directly interact with the framework. Power spectra derived from trajectories for SOMS models with a monovalent ion like Na^+ exhibit peaks representing equivalent pore environments in both the SOMS and the Ti-doped SOMS structures.

4. Conclusion

We are using a variety of different analytical techniques to help elucidate the role of occluded water in ion exchange selectivity of molecular sieves, in particular, the SOMS. INS has allowed us to probe the nature of hydrogen bonding of water molecules in the SOMS materials. INS shows that in the low selectivity as-synthesized end member, the water exhibits an ice-like extended hydrogen-bonding nature. The ^1H MAS NMR data confirms the INS data, that there is a great difference in the mobility between the $Na_2Nb_2O_6 \cdot H_2O$ end member (low selectivity) and the $Na_2Nb_{1.6}Ti_{0.4}O_{5.6}(OH)_{0.4} \cdot H_2O$ material (high selectivity). The occluded water molecules in the end member are very rigid, almost immobile. This is in contrast to the water molecules of the 20% Ti SOMS where they have very high mobility. It appears that in molecular sieves in which the water is mobile, there is a cation solvation effect associated with the water, thereby allowing greater mobility of the cation. Contrary to this, when there is little water mobility, the cation is locked into its crystallographic site while the water is forming relatively rigid hydrogen bonding with itself throughout the channels. In both the 20% Ti−SOMS and the Sr-exchanged samples, the effective free volumes of the pores are decreased. This is due to cation size and charge balancing framework $-O_fH$ molecules present in the pore. The result is a disruption of the extended H-bonding network, further resulting in the disruption of possibly "ice-like" structural formations. Ongoing studies are focused on studies of the occluded water molecules in heavily hydrated zeolite systems with overall high ion-exchange capacities. Furthermore, we are further developing and greatly expanding our research with molecular dynamics simulations involving a full exploration of the power spectra of occluded water molecules.[36]

Acknowledgment. Sandia is a multiprogram laboratory operated by Sandia Corporation, a Lockheed Martin Company, for the U.S. Department of Energy's (DOE) National Nuclear Security Administration under Contract No. DE-AC04-94AL85000. This work has benefited from the use of the Manuel Lujan, Jr. Neutron Scattering Center at LANSCE, which is funded by the Department of Energy's Office of Basic Energy Sciences. Los Alamos National Laboratory is operated by Los Alamos National Security LLC under DOE Contract No. DE-AC52-06NA25396.

Supporting Information Available: ^{1}H MAS NMR spectra of $Na_2Nb_2O_6 \cdot H_2O$ and $Na_2Nb_{1.6}Ti_{0.4}O_{5.6}(OH)_{0.4} \cdot H_2O$. This material is available free of charge via the Internet at http://pubs.acs.org.

References and Notes

(1) Klafter, J.; Blumem, A.; Drake, J. M. *Relaxation and Diffusion in Restricted Geometry*; Klafter, J., Drake, J. M., Eds.; Wiley: New York, 1989.

(2) Arndt, M.; Stannarius, R.; Gorbatschow, W.; Kremer, R. *Phys. Rev. E: Stat. Phys., Plasmas, Fluids, Relat. Interdiscip. Top.* **1996**, *54*, 5377.

(3) (a) Breck, D. W. *Zeolite Molecular Sieves;* Wiley: New York, 1974. (b) Sherry, H. S. Ion Exchange. In *Handbook of Zeolite Science and Technology;* Auerbach, S. M., Carrado, K. A., Dutta, P. K., Eds.; Marcel Dekker: New York, 2003.

(4) (a) Yang, S. Y.; Navrotsky, A.; Wilkin, R. *Am. Mineral.* **2001**, *86*, 438. (b) Sun, P. P.; Deore, S.; Navrotsky, A. *Microporous Mesoporous Mater.* **2006**, *91*, 15.

(5) Corsaro, C.; Crupi, V.; Majolino, D.; Parker, S. F.; Venuti, V.; Wanderlingh, U. *J. Phys. Chem. A* **2006**, *110*, 1190.

(6) Hunger, J.; Beta, I. A.; Bohlig, H.; Ling, C.; Jobic, H.; Hunger, B. *J. Phys. Chem. B* **2006**, *110* (1), 342.

(7) Beta, I. A.; Bohlig, H.; Hunger, B. *Phys. Chem. Chem. Phys.* **2004**, *6*, 1975.

(8) Crupi, V.; Majolino, D.; Migliardo, P.; Venuti, V.; Wanderlingh, U.; Mizota, T.; Telling, M. *J. Phys. Chem.* **2004**, *108*, 4314.

(9) Jobic, H.; Tuel, A.; Krossner, M.; Sauer, J. *J. Phys. Chem.* **1996**, *100*, 19545.

(10) Line, C. M. B.; Kearley, G. J. *J. Chem. Phys.* **2000**, *112*, 9058.

(11) Higgins, F. M.; de Leeuw, N. H.; Parker, S. C. *J. Mater. Chem.* **2002**, *12*, 124.

(12) (a) Nyman, M. D.; Tripathi, A.; Parise, J. B.; Maxwell, R. S.; Harrison, W. T. A.; Nenoff, T. M. *J. Am. Chem. Soc.* **2001**, *123*, 1529. (b) Nyman, M. D.; Tripathi, A.; Parise, J. B.; Maxwell, R. S.; Nenoff, T. M. *J. Am. Chem. Soc.* **2002**, *124*, 1704. (c) Nenoff, T. M.; Nyman M. Niobate-based octahedral molecular sieves. U.S. Patent 6,596,254, 2003.

(13) Pless, J. D.; Garino, T. J.; Maslar, J. E.; Nenoff, T. M. *Chem. Mater.* **2007**, in press.

(14) JCPDS, Joint Committee of Powder Diffraction Standards database, International Centre for Diffraction Data (ICDD).

(15) Holland, G. P.; Cherry, B. R.; Alam, T. M. *J. Magn. Reson.* **2004**, *167*, 161.

(16) Alam, T. M.; Nyman, M.; Cherry, B. R.; Segall, J. M.; Lybarger, L. E. *J. Am. Chem. Soc.* **2004**, *126*, 5610.

(17) Alam, T. M.; Nyman, M.; McIntyre, S. K. *J. Phys. Chem. A* **2007**, *111*, 1792.

(18) Alam, T. M.; Pless, J. D.; Nenoff, T. M. Probing Water Dynamics in Octahedral Molecular Sieves: High Speed ^{1}H MAS NMR Investigations. In *Magnetic Resonance in Material Science;* Herberg, J., Wu, Y., Grandinetti, P., Hayes, S., Farnan, I., Eds.; Mater. Res. Soc. Symp. Proc. 984E: Warrendale, PA, 2007; 0984-MM03-03.

(19) Perdew, J. P.; Burke, K.; Ernzerhof, M. *Phys. Rev. Lett.* **1996**, *77*, 3865.

(20) Blochl, P. E. *Phys. Rev. B* **1994**, *50*, 17953.

(21) Kresse, G.; Joubert, D. *Phys. Rev. B* **1999**, *59*, 1758.

(22) Kresse, G.; Furthmuller, J. *Phys. Rev. B* **1996**, *54*, 11169; *Comp. Mater. Sci.* **1996**, *6*, 15.

(23) Berendsen, H. J. C.; Postma, J. P. M.; van Gunsteren, W. F.; Hermans, J. Interaction models for water in relation to protein hydration. In *Intermolecular Forces;* Pullman, B., Ed.; Reidel: Dordrecht, Holland, 1981; p 331.

(24) Teleman, O.; Jonsson, B.; Engstrom, S. *Mol. Phys.* **1987**, *60* (1), 193.

(25) Åqvist, J. *J. Phys. Chem.* **1990**, *94*, 8021.

(26) Halgren, T. A. *J. Am. Chem. Soc.* **1992**, *114* (20), 7827.

(27) Frenkel, D.; Smit, B. *Understanding Molecular Simulations: From Algorithms to Applications*, 2nd ed.; Academic Press: San Diego, CA, 2002.

(28) Rietveld, H. M. *J. Appl. Crystallogr.* **1969**, *2*, 65.

(29) Larson, A. C.; Von Dreele, R. B. *GSAS-General Structure Analysis System*; Los Alamos National Laboratory: Los Alamos, NM, 2000; Los Alamos National Laboratory Report No. LAUR 86-748.

(30) Nenoff, T. M.; Ockwig, N. W.; Pless, J. D.; Alam, T. M.; Hartl, M. A.; Daemon, L. L. *Stud. Surf. Sci. Catal.* **2007**, submitted.

(31) Li, J-C.; Kolesnikov, A. I. *J. Mol. Liq.* **2002**, *100/1*, 1.

(32) Corsaro, C.; Crupi, V.; Longo, F.; Majolino, D.; Venuti, V.; Wanderlingh, U. *J. Phys.: Condens. Mater.* **2005**, *17*, 7925.

(33) Bopp, P. *Pure Appl. Chem.* **1987**, *59*, 1071.

(34) Marti, J. *J. Chem. Phys.* **1999**, *110*, 6876.

(35) Bougeard, D.; Smirnov, K. S. *Phys. Chem. Chem. Phys.* **2007**, *9*, 226.

(36) Ockwig, N. W.; Cygan, R. T.; Criscenti, L. J.; Nenoff, T. M. *Phys. Chem. Chem. Phys.* **2007**, submitted.